Rydberg-atom masers. I. A theoretical and experimental study of super-radiant systems in the millimeter-wave domain

L. Moi,* P. Goy, M. Gross, J. M. Raimond, C. Fabre, and S. Haroche
Laboratoire de Physique de l'Ecole Normale Superieure
24 rue Lhomond, 75231 Paris Cedex 05, France
(Received 16 March 1982)

The operation of maser devices using highly excited Rydberg atoms as active medium is investigated. These systems, working in a transient regime reminiscent of super-radiance generate few-hundred-ns-long bursts of mm-wave radiation. They are characterized by extremely low inversion density thresholds ($N_0 \sim 10^4$ atoms typically) and very small peak power outputs (in the 10^{-11}- to 10^{-13}-watt range). This study is interesting in the context of new tests of super-radiance and electrodynamics theory. It also opens new possibilities in the important domain of mm-wave amplification and detection. In this paper, we present a simple semiclassical theory of transient Rydberg maser operation and we report the experimental observation of a large number of maser emission lines on Na atoms, spanning a wide frequency interval ($60 < \nu < 950$ GHz). The technique used to monitor the emission is the indirect field ionization procedure which reveals fast radiative transfers occurring between Rydberg levels. Another method involving the direct detection of the maser radiation by a heterodyne receiver is described in a subsequent paper, along with a report on the investigation of various effects related to the triggering of the transient maser emission by external radiation.

I. INTRODUCTION

Rydberg atoms are bound atomic systems in which a valence electron has been excited in a level of very high principal quantum number n. Energy intervals between Rydberg levels with adjacent n values are of the order of $e^2/4\pi\epsilon_0 a_0 n^3$ (a_0, Bohr radius; e, electron charge) and fall in the millimeter- (mm) wave domain for $n \sim 20$ to 50. The electric dipole matrix elements between neighbor Rydberg levels which measures the strength of the atom-field coupling are of the order of $ea_0 n^2$ and, for $n \sim 20$ to 50, turn out to be about three orders of magnitude larger than in "ordinary" (i.e., low excited) atomic systems. As a result, Rydberg atoms ($n \sim 20$ to 50) interact resonantly and very strongly with millimeter-wave radiation. Ensembles made of relatively small numbers of such atoms, conveniently excited by short laser pulses, behave as transient amplifiers of microwave radiation and can be used as active medium in maser systems exhibiting quite interesting characteristics.

The principle of these masers is sketched in Fig. 1. An atomic beam (Na atoms in our experiments) crosses a mm-wave cavity (finesse ≥ 100) made of two parallel mirrors. This beam is excited by a short (few ns duration) laser pulse in a Rydberg level (usually an $nS_{1/2}$ state). Immediately after the

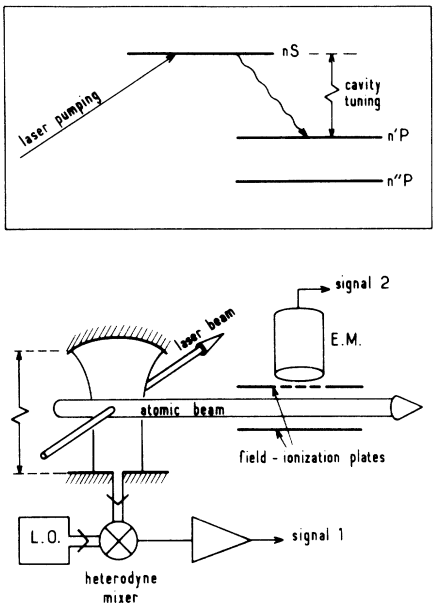

FIG. 1. General scheme of Rydberg-atom maser. Signal 1 corresponds to the direct detection of the microwave emitted by the atoms. Signal 2 is an indirect detection consisting in measuring the radiative atomic population transfers through field ionization of the Rydberg atoms. (In the insert: Energy levels relevant for maser emission. The final $n'P$ state of the emission is selected by cavity tuning.)

laser pulse, the atomic medium is totally inverted on all the transitions connecting the initial Rydberg level to more bound states. If the cavity is tuned to the frequency of one of these transitions [usually $nS_{1/2} \rightarrow (n-1)P_{1/2,3/2}$ or $nS_{1/2} \rightarrow (n-2)P_{1/2,3/2}$] and if the population inversion is larger than a given threshold [$\sim 10^4$ atoms for an $nS_{1/2} \rightarrow (n-1)P_{1/2}$ transition with $n \sim 30$], the inverted medium emits a short burst of radiation and decays within a few hundred ns to the lower state of the transition. The emission process can be detected either directly by recording the microwave signal or indirectly by monitoring the fast atomic population transfer. The first detection method is performed with the help of a mm-wave heterodyne receiver coupled to the cavity through a waveguide and requires a reference signal from a local oscillator (LO). For the second method the Rydberg atoms are ionized, after they have left the cavity, with the help of an electric field pulse produced by two parallel condenser plates. The resulting electrons are detected with an electron multiplier. The threshold electric field for ionizing the atoms depends on their excitation, which enables one to discriminate in the ionization current the contributions from the upper and the lower states of the maser transition and thus to measure the radiative population transfer.

The interest in these experiments is twofold. (i) Fundamentally, these Rydberg systems operate in a transient regime reminiscent of the Dicke superradiance phenomenon,[1] some aspects of which can be studied for the first time with these new devices. Two features, in particular, make these superradiant sources quite unique: They operate at very long wavelengths (as compared to other atomic systems) and the emission thresholds are exceedingly low. The first property makes it possible to realize active atomic media whose size is of the order of or even smaller than the emission wavelength. One can then study interesting size sample effects much more easily than in the near-infrared or in the optical domains. On the other hand, the low threshold property, which reflects the very large size of the Rydberg-atom electric dipoles, makes it possible to contemplate realistic situations where a few excited atoms only would emit coherently in the mm-wave cavity. Investigation of such systems, at the boundary between microscopic and macroscopic electrodynamics, is certainly very promising. (ii) On a more applied level, these Rydberg systems provide a new way of amplifying and detecting millimeter waves in an extended frequency domain. The range of possible masing frequencies is indeed quite large due to the great density of Rydberg levels lying in a few-thousand-GHz-frequency bandwidth below the ionization limit of the active atoms. The very large atom mm-wave field coupling makes these amplifiers very sensitive and potentially able to detect single photons, a quite unusual performance in the mm-wave domain.

In this and in a subsequent article, we present the results of our present investigations on these systems, the preliminary results of which have been reported in previous publications.[2-5] This paper gives a simple theoretical analysis of the transient Rydberg-maser operation and describes the recently performed observations of maser signals on transitions between Na Rydberg states. In the subsequent paper, we will discuss the important problem of the "triggering" of the maser emission. Usually, such devices are triggered by the blackbody radiation background. We will study how the maser emission characteristics depend on this background temperature. We will also show how a small mm-wave "external" signal added to this background can alter the maser emission and how this effect can precisely be used to amplify and detect the mm-wave radiations.

The outline of this first paper will be as follows. In Sec. II, we present a semiclassical description of the transient Rydberg-maser operation. We then turn to the description of our experimental setup (Sec. III), with a detailed analysis of one of the two possible detection procedures. (We only describe here the indirect detection method involving the atomic field ionization and we leave the description of the direct heterodyne detection method for the next article.) The detailed observation of the maser emission on the $33S \rightarrow 32P$ transition in Na, chosen as a typical example, is presented in Sec. IV. Various effects predicted by the model of Sec. II have been observed on this transition and are described in Sec. IV. We then present in Sec. V the ensemble of transitions on which similar maser effects have been observed. We also briefly describe the observation of various line competition, quenching, and cascading transition effects which result from the complex level structure of the emitting Rydberg atoms. At last, in Sec. VI, we report the measurement of very low inversion thresholds and we discuss the possibility of realizing similar devices with only one (or few) Rydberg atoms, which would constitute new interesting tests of electrodynamics.

II. THEORY OF THE TRANSIENT RYDBERG MASER

We are interested here in the description of the evolution of an ensemble of Rydberg atoms

prepared by a short excitation in a given initial state and placed in an open Fabry-Perot resonator. We will show that, in simple cases at least, this problem might reduce to the emission of an ensemble of two-level atoms interacting with a single cavity mode. This problem has already been studied in the context of transient super-radiant and laser systems[6] and two different evolution regimes have been predicted: If the cavity damping time is short enough, the atoms emit a single burst of radiation; on the other hand, if the cavity has a large enough quality factor, the emission shows up a succession of secondary bursts, or ringings, corresponding to an oscillatory exchange of energy between the atoms and the field. A point which has been, to our knowledge, not considered so far is that the system evolution also depends, in both of the above mentioned regimes, upon the size of the active medium in the cavity. If this size is smaller than the emission wavelength λ, the upper atomic level population is totally depleted at the end of the evolution (π pulse emission). If, on the other hand, the medium extends over many wavelengths, the upper level is only partially emptied and, after the emission has ended, a fraction of the total number of atoms remains excited (partial or limited emission). This effect can only be understood by a proper description of the standing wave pattern of the field in the cavity. In the domain of Rydberg-atom emission, where the wavelength λ is relatively large (mm- or cm-wave domain), this sample size effect is particularly important and has indeed been put in evidence in our experiments. We thus find it justified to give here a brief theoretical description of the Rydberg-maser evolution taking this effect into account. This description will also allow us to point out the similitude between the Rydberg emission process occurring in a resonant cavity and super-radiant emission of atoms in free space. We will see that the equations governing the atomic evolution are in both cases basically equivalent and that the presence of the cavity, by imposing its simple mode structure to the atoms, considerably simplifies the intricate geometrical and propagation effects which constitute unessential complications to the analysis of super-radiance in free space.

The material of this theoretical section is organized as follows: In Sec. II A, we show how the Rydberg emission can, in a simple case, be reduced to a two-level atom problem. We define, then, the various parameters relevant to the analysis of the atom and field evolution (Sec. II B) and we write the coupled Bloch-Maxwell equations which, in the semiclassical formalism, describe this evolution (Sec. II C). A very simple representation of these equations in term of the so-called Bloch angle is recalled in Sec. II D. Section II E defines the initial conditions of the system evolution. We briefly indicate here how one can describe, in the semiclassical treatment, the quantum and blackbody radiation fluctuations responsible for the onset of the emission process (a detailed analysis of the initial stage of the emission will be given in the second paper of this series). In Sec. II F, we indicate the general form of the solutions of the Bloch-Maxwell equations with the help of a classical analogy assimilating the system to a pendulum. The two limiting regimes discussed above (damped and oscillatory behavior) are briefly described. In Sec. II G, we emphasize the analogy of the damped regime with super-radiant emission in free space. Section II H discusses the size sample effects mentioned above. We then proceed to the evaluation of the maser threshold condition (Sec. II I). Sections II J and II K are devoted to the brief analysis of effects which cannot be accounted for by the two-level atom model; the polarization of the emitted radiation is described in a simple case in Sec. II J and some competition, quenching, and cascading emission effects are discussed in Sec. II K.

A. Reduction to a two-level atom problem

The initially inverted system can *a priori* emit on a large number of competing transitions connecting the initial state to more bound ones. However, if the cavity is tuned to the frequency ω associated to one of these transitions, it considerably enhances the field components "seen" by the atoms at this frequency and speeds up the system evolution towards the corresponding final state. The other atomic transition rates can then, in general, be neglected and the Rydberg atom can be described as a single-transition system (the precise validity condition for this approximation will be given in Sec. II K, after we have established the solution in the two-level atom case).

Another slight complication might also arise from the degeneracy of the levels involved in the transition. To be specific, the situation we have in mind in this section (except for Sec. II K) concerns the initial excitation of an $nS_{1/2}$ state in sodium, the cavity being tuned in resonance with an $nS_{1/2} \rightarrow n'P_{1/2}$ transition. In this case, the initial and final states have both a $J=\frac{1}{2}$ angular momentum and each decomposes in two degenerate $m_J=+\frac{1}{2}$ and $m_J=-\frac{1}{2}$ magnetic sublevels (see

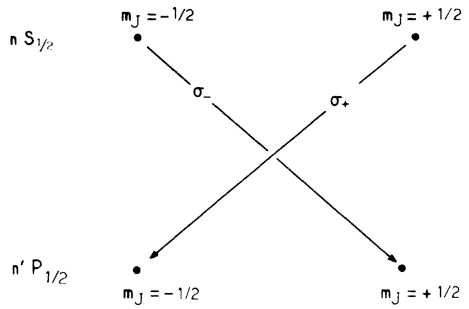

FIG. 2. Level scheme relevant to the $nS_{1/2} \rightarrow n'P_{1/2}$ maser emission. Two σ_+ and σ_- components are radiated independently by two uncoupled groups of atoms.

Fig. 2). (The coupling of the electron with the nuclear spin of the alkali, giving rise to the hyperfine structure, can in this problem be neglected since the corresponding energy splittings are in Na of the order of tens of kHz only. The maser emission time scale, of the order of a fraction of microsecond, is too short for this coupling to appreciably perturb the electronic motion.) The quantization axis being chosen along the Oz direction of the cavity axis, it is clear that the only two electromagnetic field polarizations the cavity can sustain are the circular polarizations σ_+ and σ_- corresponding, respectively, to the $nS_{1/2}$, $m_J = +\frac{1}{2} \rightarrow n'P_{1/2}$, $m_J = -\frac{1}{2}$, and $nS_{1/2}$, $m_J = -\frac{1}{2} \rightarrow n'P_{1/2}$, $m_J = +\frac{1}{2}$ transitions,

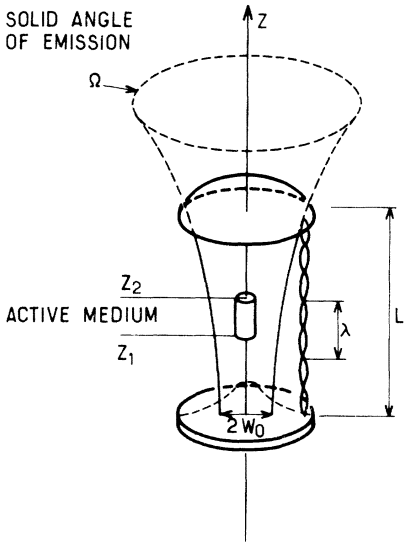

FIG. 3. Schematics of the Fabry-Perot resonator with indication of its relevant geometric parameters and the position of the active medium.

respectively (arrows on the figure). As long as no coherence is initially introduced between the two $m_J = -\frac{1}{2}$ and $m_J = +\frac{1}{2}$ substates of the $nS_{1/2}$ level, it is obvious that these two transitions concern two independent classes of atoms and two independent electromagnetic field components. The system can thus be described as a superposition of two two-level atom subsystems evolving independently (of course, the two independently emitted field components add up on the detector, as will be discussed in Sec. II J). As a result, the calculation of the Rydberg-atom emission reduces in this simple case to a two-level atom problem. Of course, more complex situations, in which the degeneracies of the levels involved in the transition are higher, might also be considered (for example, $nD \rightarrow n'P$ transitions). These cases do not reduce to two-level problems and might give rise to interesting polarization effects of the emitted radiation. We will not discuss these problems here.[7,8]

B. Description of the system and notations

1. The cavity

The cavity (see Fig. 3) is an open Fabry-Perot resonator of length L ($L \gg \lambda$), which is resonant for the atomic transition frequency $\omega = (2\pi c)/\lambda = ck$. We assume that it sustains only one Gaussian mode, having a waist w_0. The mirrors having a high reflectivity R, the cavity finesse f

$$[f = \pi\sqrt{R}/(1-R)]$$

can be written as

$$f \approx \frac{\pi}{1-R} . \tag{1}$$

The characteristic damping time of the energy in the cavity is

$$T_{\text{cav}} = \frac{f}{\pi}\frac{L}{c} . \tag{2}$$

It will also be convenient for the description to follow to introduce the dimensionless μ coefficient

$$\mu = \frac{3}{4\pi^2}\frac{\lambda^2}{w_0^2} . \tag{3}$$

This factor is equal to the μ coefficient[9] introduced in the super-radiance theory $\mu = 3\lambda^2/8\pi S$ when replacing the active medium transverse area S by the energy mode area at the the waist $S = \frac{1}{2}\pi w_0^2$. It is also proportional to the diffraction-limited solid an-

gle Ω of the cavity mode.

The time it takes to establish a standing wave in the cavity is of the order of L/c, which we will assume to be much shorter than all other evolution times in the problem. As a result, the field in the cavity can always be described as a standing wave. Along the z axis of the cavity, the envelope of the field is expressed as

$$\mathcal{E}(z,t)=\mathcal{E}_0(t)\cos kz \tag{4}$$

(the two mirrors corresponding to z values such that $\cos kz=0$).

2. *Shape and position of the atomic sample*

The active medium, made of N_0 two-level atoms, fills a small cylinder in the cavity, coaxial to it, with transverse dimensions much smaller than the mode waist w_0 (see Fig. 3). The two end planes of the cylinder have abscissas z_1 and z_2. The atoms in plane z ($z_1 \le z \le z_2$) all "see" a field envelope given by Eq. (4).

3. *Atomic system*

The two-level atoms are resonant on a nondegenerate mm-wave transition between levels $|a\rangle$ and $|b\rangle$, at angular frequency ω (see Fig. 4). They are initially prepared (time $t=0$) in the upper level $|a\rangle$ by a short laser pulse exciting them from the atomic ground state (not shown on the figure). The electric dipole matrix element $\langle a|D|b\rangle=d$ between states $|a\rangle$ and $|b\rangle$ is assumed to be real. We call

$$\Gamma=\frac{\omega^3 d^2}{3\pi\epsilon_0\hbar c^3} \tag{5}$$

the partial spontaneous emission decay rate from level $|a\rangle$ to $|b\rangle$. Typically, $d\sim ea_0n^2$ is of the order of 500 a.u. for Rydberg transitions around $n\sim 30$. Transition frequencies $\nu=\omega/2\pi$ being in the 100-GHz range, this corresponds to partial decay rate Γ of the order of 20 s^{-1}. In spite of the huge electric dipoles, this value is very small compared to an optical spontaneous emission rate because of the ω^3 dependence of Γ.

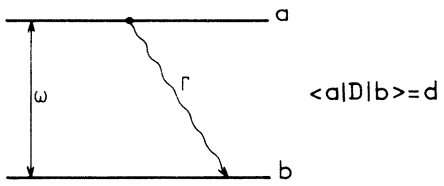

FIG. 4. Two-level atom has a dipole matrix element d and a partial radiation decay rate from $|a\rangle$ to $|b\rangle$ equal to Γ.

It is convenient to introduce the local population difference density $\mathcal{N}(z,t)$ and polarization density $\mathcal{P}(z,t)$ of atoms in plane z at time t. Calling ρ^i the density matrix of atom i ($1\le i\le N_0$) and arbitrarily dividing the z axis in small Δz intervals ($\Delta z \ll \lambda$), we define these local quantities as

$$\mathcal{N}(z,t)=\frac{1}{\Delta z}\sum_{i\in[z,z+\Delta z]}[\rho_{aa}^{(i)}(t)-\rho_{bb}^{(i)}(t)] , \tag{6a}$$

$$\mathcal{P}(z,t)=\frac{d}{\Delta z}\sum_{i\in[z,z+\Delta z]}\rho_{ab}^{(i)}(t)e^{i\omega t} . \tag{6b}$$

Other useful quantities are the average population inversion and polarization per atom, $n_a(t)$ and $p_a(t)$ given by

$$n_a(t)=\frac{1}{N_0}\int_{z_1}^{z_2}\mathcal{N}(z,t)dz , \tag{7a}$$

$$p_a(t)=\frac{1}{N_0}\int_{z_1}^{z_2}\mathcal{P}(z,t)dz . \tag{7b}$$

C. Bloch-Maxwell equations describing the atom-field evolution

In the semiclassical theory of radiation, the evolution of $\mathcal{N}(z,t)$ and $\mathcal{P}(z,t)$ in the field $\mathcal{E}_0(t)\cos kz$ are given by the so-called Bloch equations[7,10]:

$$\frac{d}{dt}\mathcal{P}(z,t)=\frac{id^2}{\hbar}\mathcal{E}_0(t)\mathcal{N}(z,t)\cos kz , \tag{8a}$$

$$\frac{d}{dt}\mathcal{N}(z,t)=\frac{i}{2\hbar}[\mathcal{E}_0^*\mathcal{P}(z,t)-\mathcal{E}_0\mathcal{P}^*(z,t)]\cos kz . \tag{8b}$$

We neglect here all relaxation mechanisms which damp the atomic observables (collisions, escape of the atoms from the cavity, etc.); we, indeed, assume that the radiative damping of the atoms coupled to the cavity is much faster than all these other relaxing mechanisms. (Relaxation will only be introduced in Sec. II I to calculate the maser threshold.)

Equations (8) clearly show that each class of atom (corresponding to a given z value) evolves according to its own rate, depending on the value of $\cos kz$. Atoms located at nodes of the cavity mode ($\cos kz=0$) do not evolve at all, whereas atoms at antinode positions ($\cos kz=\pm 1$) undergo the fastest evolution. These equations have to be completed by

the equation describing the evolution of the field envelope $\mathscr{E}_0(t)$. An easy way to obtain it is to express the energy conservation for the combined atoms and field system. At time t, the energies W_A and W_R, respectively, stored in the atoms and in the field are

$$W_A=\frac{\hbar\omega}{2}N_0 n_a=\frac{\hbar\omega}{2}\int_{z_1}^{z_2}\mathscr{N}(z,t)dz\ , \tag{9a}$$

$$W_R=\epsilon_0\frac{\pi w_0^2 L}{8}\,|\,\mathscr{E}_0(t)\,|^2\ . \tag{9b}$$

The time variation of the electromagnetic energy is due to cavity losses and to the energy flow from the atoms:

$$\frac{dW_R}{dt}=-\frac{W_R}{T_{\text{cav}}}-\frac{\hbar\omega}{2}\int_{z_1}^{z_2}\frac{d\mathscr{N}(z,t)}{dt}dz\ . \tag{10}$$

Replacing in Eq. (10) W_R and

$$\frac{d\mathscr{N}(z,t)}{dt}$$

by their expressions (9b) and (8b), one immediately gets

$$\frac{d\mathscr{E}_0}{dt}=-\frac{\mathscr{E}_0}{2T_{\text{cav}}}-\frac{2i\omega}{\epsilon_0\pi W_0^2 L}\int_{z_1}^{z_2}\mathscr{P}(z,t)\cos kz\,dz\ . \tag{11}$$

The set of so-called Bloch-Maxwell equations (8a), (8b), and (11) allows us to calculate the coupled evolution of $\mathscr{E}_0(t)$, $\mathscr{P}(z,t)$, and $\mathscr{N}(z,t)$. It is clear that the initial conditions of the system evolution at time $t=0$:

$$\mathscr{E}_0(z,0)=0,\quad \mathscr{P}(z,0)=0\ ,$$

$$\mathscr{N}(z,0)=N_0\frac{1}{z_2-z_1}\ ,$$

correspond to an unstable equilibrium state for the solutions of the Bloch-Maxwell equations. In order to describe the departure of the system from this state, one has to introduce *ad hoc* fluctuations simulating the random fields (spontaneous emission and blackbody radiation) impinging on the system at time $t=0$. Before recalling the now standard procedure used to describe these fluctuations, let us first give a very convenient geometric representation of the Bloch-Maxwell equations. To initiate the system, we will simply consider that the initial value of the polarization density $\mathscr{P}(z,0)$ is very small, but nonzero.

D. Bloch angle representation

A two-level atom located at point z can be represented in a standard way as a fictitious spin $\frac{1}{2}$ system. In this analogy, the upper and lower states $|a\rangle$ and $|b\rangle$ correspond to the spin states $|\pm\frac{1}{2}\rangle$ pointing along an arbitrary quantization direction in an abstract space. The atomic state at time t, which is a linear superposition of $|a\rangle$ and $|b\rangle$ is then represented as a spin pointing in a direction defined by a polar angle $\theta(z,t)$ and an azimuthal angle $\phi(z,t)$ with respect to this axis. $\mathscr{N}(z,t)$ and $\mathscr{P}(z,t)$ are readily expressed as functions of θ and ϕ:

$$\mathscr{N}(z,t)=\frac{1}{z_1-z_2}N_0\cos\theta(z,t)\ , \tag{12a}$$

$$\mathscr{P}(z,t)=\frac{i}{z_1-z_2}N_0 d e^{i\phi(z,t)}\sin\theta(z,t)\ . \tag{12b}$$

Replacing $\mathscr{N}$ and $\mathscr{P}$ by their expressions in Eqs. (8) and using the fact that $\mathscr{P}(z,0)$ is very small, one gets

$$\frac{d}{dt}\theta(z,t)=\frac{d}{\hbar}[\mathscr{E}_0(t)e^{-i\phi}]\cos kz\ , \tag{13a}$$

$$\frac{d}{dt}\phi(z,t)=0\ , \tag{13b}$$

$\theta(z,t)$ being real in (13a), $\mathscr{E}_0(t)\exp[-i\phi(z,t)]$ is also real and, therefore,

$$\frac{d}{dz}\phi(z,t)=0\ . \tag{13c}$$

The phase ϕ of the polarization density $\mathscr{P}(z,t)$ is then the same as the phase of the complex field amplitude and is independent of z and t. This puts strong restrictions to the spatial and time variations of the atomic polarization phase in the active medium.

$\theta(z,t)$, which starts from a very small value $\theta(z,0)$, becomes very quickly proportional to $\cos kz$, so that one has

$$\theta(z,t)=\theta_0(t)\cos kz \tag{14}$$

with

$$\frac{d\theta_0(t)}{dt}=\frac{d}{\hbar}[\mathscr{E}_0(t)e^{-i\phi}]\ . \tag{15}$$

The average population inversion per atom is also readily expressed in terms of $\theta_0(t)$ from Eqs. (7a) and (12a):

$$n_a(t)=\frac{1}{z_1-z_2}\int_{z_1}^{z_2}\cos[\theta_0(t)\cos kz]dz\ . \tag{16}$$

Finally, after some straightforward calculations, the Maxwell equation (11) can be rewritten as

$$\frac{d^2\theta_0}{dt^2}+\frac{1}{2T_{\rm cav}}\frac{d\theta_0}{dt}+2\Gamma N_0\mu\frac{c}{L}\frac{dn_a}{d\theta_0}=0\ , \tag{17}$$

where Γ and μ are defined by Eqs. (3) and (5). This equation is very similar to the one derived in Ref. 6.

Solving Eq. (17) with the *ad hoc* initial conditions described in Sec. II E yields $\theta_0(t)$ and hence the time evolution of the electric field, atomic population, polarization, and energy through Eqs. (15), (12), and (9a). Equation (17) can be given a very simple interpretation. It represents the motion of a damped particle in a potential well proportional to $n_a(\theta_0)$, i.e., to the atomic average energy. The second term in Eq. (17) describes, indeed, a viscous drag proportional to the particle "velocity" and the last term has the form of a "force" deriving from this potential and acting on the particle.

The shape of the potential is given by Eq. (16). It depends obviously on the position and extension of the atomic slab z_1-z_2 across the standing wave pattern of the cavity mode. Plots of this potential well for two typical values of z_1-z_2 are shown on Fig. 5. Figure 5(a) corresponds to $|z_1-z_2|\ll\lambda$, the case of a "small" sample centered around an antinode position in the cavity. One then has

$$\cos(\theta_0\cos kz)\simeq\cos\theta_0$$

and $n_a(\theta_0)$ reduces to

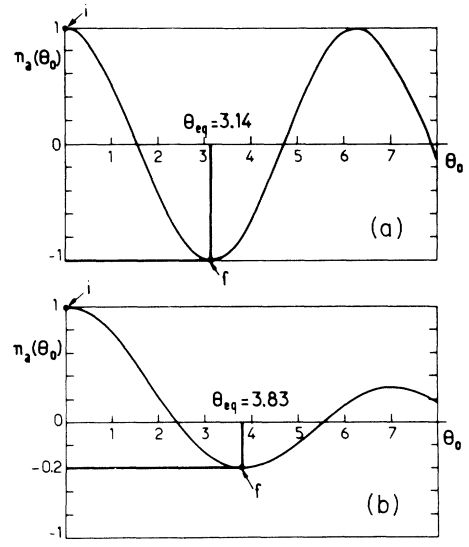

FIG. 5. "Potential wells" $n_a(\theta_0)$ governing the evolution of the Bloch angle θ_0. (a) Small sample case $|z_1-z_2|\ll\lambda$; (b) large sample case $|z_1-z_2|\geq\lambda$. Arrows i and f indicate in each case the initial and final positions of the system.

$$n_a(\theta_0)=\cos\theta_0\ . \tag{18}$$

Figure 5(b) corresponds, on the other hand, to $|z_1-z_2|=\lambda$ or $|z_1-z_2|\gg\lambda$, the sample being again centered at a field maximum. In that case, the integral in Eq. (16) reduces to the zeroth-order Bessel function

$$n_a(\theta_0)=J_0(\theta_0)\ . \tag{19}$$

For sample extending over a fractional number of wavelengths, the $n_a(\theta)$ variation is "intermediate" between the two curves of Figs. 5(a) and 5(b). In all cases, it exhibits oscillations with an infinite number of potential maxima and minima. The initial condition $\theta_0=0$, always corresponds to a maximum and hence to an unstable equilibrium for the system. We now recall how to describe the departure from this unstable position.

E. Description of the initial quantum fluctuations (Refs. 11–13 and 7)

The initial value of θ_0 at time $t=0$ and the value of ϕ should be chosen as random quantities θ_0^i,ϕ^i reflecting the quantum fluctuations of the electromagnetic field which triggers the atom polarization away from its $\theta_0=0$ initial state. If the maser starts on spontaneous emission alone (zero temperature of the maser cavity), the probability laws for ϕ^i and θ_0^i are[7]

$$P(\phi^i)=\frac{1}{2\pi}\ , \tag{20}$$

$$P(\theta_0^i)=\frac{2\theta_0^i}{\bar\theta^2}\exp\left[-\left[\frac{\theta_0^i}{\bar\theta}\right]^2\right]\ , \tag{21}$$

with $\bar\theta$ being the mean square root value of the initial Bloch Angle (tipping angle) being given by[6,11]

$$\bar\theta=\frac{2}{\sqrt{N_0}}\ . \tag{22}$$

Equations (20) and (21) express that the initial polarization obeys a Gaussian statistics with a totally random phase equally distributed between 0 and 2π. Two maser pulses corresponding to the same atomic preparation (same number N_0 of initially inverted atoms) will have different $\theta_0(t)$ evolutions due to the different choices of initial values for θ_0^i. Pulse to pulse fluctuations are described by the probability law (21). We will call "average evolution" the one corresponding to the average initial condition $\theta_0(0)=\bar\theta$.

The above results are slightly modified if the cav-

ity has a nonzero temperature T. In that case, the initial fluctuations are of thermal origin (blackbody radiation). We will show in the second paper of this series that the probability law for θ^i remains Gaussian with a new mean value

$$\bar{\theta}(T)=\frac{2}{\sqrt{N_0(T)}} \tag{23a}$$

with

$$N_0(T)=\frac{N_0}{1+\bar{n}_B}\ , \tag{23b}$$

where

$$\bar{n}_B=\left[\exp\left[\frac{\hbar\omega}{k_BT}\right]-1\right]^{-1} \tag{23c}$$

is the average blackbody photon number per cavity mode.

Starting from its small θ_0^i initial value, the pseudoparticle describing the maser evolution will roll down the potential well represented on Fig. 5 and the pulse intensity, proportional to the kinetic energy of the particle, will rapidly increase. We briefly describe in Sec. II F the main features of the system evolution which can easily be deduced from this simple analogy.

F. Qualitative analysis of the maser evolution: Damped and oscillatory regimes

The above geometrical representation allows us to discuss qualitatively in a very simple way the system evolution. It is clear that if the damping is large (short enough $T_{\rm cav}$), the pseudoparticle will roll down towards the first minimum of the potential well and stabilize at this point. The field intensity, proportional to $(d\theta_0/dt)^2$ will be emitted in a single radiation burst. In case of small damping (long enough $T_{\rm cav}$), the particle will go beyond the first potential minimum and oscillate back and forth until it stabilizes in a minimum position. This corresponds to successive cancellations of $d\theta/dt$ and hence to the emission of successive bursts of radiation (radiation ringings). These ringings will not be described in detail here. We will simply concentrate on the damped regime which is the one corresponding to our experiments. In this regime, the viscous term

$$\frac{1}{2T_{\rm cav}}\frac{d\theta_0}{dt}$$

dominates the acceleration term $(d^2\theta_0/dt^2)$, so that Eq. (17) reduces to a first-order differential equation

$$\frac{d\theta_0}{dt}=-\frac{1}{2T_R}\frac{dn_a}{d\theta_0} \tag{24}$$

with T_R being a characteristic evolution time for the maser radiation defined as

$$T_R^{-1}=\frac{8}{\pi}f\Gamma N_0\mu\ . \tag{25}$$

Equation (24) corresponds to the regime where the damping of the field is large enough for it to be able to follow adiabatically the atomic polarization. The $(d^2\theta_0/dt^2)$ term in Eq. (17), being of the order of

$$\frac{1}{T_R}\frac{d\theta_0}{dt}\ ,$$

makes it clear that this regime occurs if the condition

$$T_{\rm cav}\lesssim T_R \tag{26}$$

is fulfilled. This condition can also be written as a condition on the cavity finesse

$$f\lesssim\frac{\pi}{2}\left[\frac{c}{2L\Gamma N_0\mu}\right]^{1/2}\ , \tag{27}$$

which, we will see in Sec. III, is fulfilled in our experiments. In case of a small active sample ($|z_1-z_2|\ll\lambda$), Eq. (24) reduces to

$$\frac{d\theta_0}{dt}=\frac{1}{2T_R}\sin\theta_0\ , \tag{28}$$

an equation already derived in Ref. 6. In the case of an extended sample ($|z_1-z_2|=\lambda$ or $|z_1-z_2|\gg\lambda$), one gets

$$\frac{d\theta_0}{dt}=\frac{1}{2T_R}J_1(\theta_0)\ . \tag{29}$$

G. Damped regime, in the small active volume case: Connection with super-radiance in free space

Let us focus in this section on the solution of the damped regime corresponding to the case of a small emitting sample. The pendulum Eq. (28) is classical in this kind of radiation problems. It appears not only in the theory of transient masers discussed here, but also in many treatments of super-radiance in free space, where the spatial variations of the electromagnetic field along the radiating sample are neglected and where it is assumed that all atoms in-

teract with the same reaction field (so-called mean-field models).[6] However, in the case of mirrorless super-radiance, this assumption is only an approximation. If the medium is large compared to the emitted wavelength, propagation is clearly an important effect. If, on the other hand, the medium size is reduced below λ, it has been shown[14] that strong diffraction and phase disruptive dipole-dipole couplings set in before super-radiance. When the atoms radiate in a cavity, on the contrary, cooperative radiation can occur even if the atoms are placed in a small volume (at an antinode position). The cavity enhancement factor does indeed speed up the super-radiance evolution without increasing the dipole-dipole couplings which would destroy super-radiance for the same sample size in free space. In other words, small sample transient masers can be considered as practical super-radiant systems where the mean-field approximation is truly fulfilled.

The connection between the transient maser operation and super-radiance in free space also appears clearly if one examines Eq. (25) giving the characteristic field evolution time T_R. For a sample made of N_0 atoms radiating in free space in a solid angle μ, the super-radiant time would merely be $(\Gamma N_0 \mu)^{-1}$. Equation (25) expresses the fact that the emission in the cavity is essentially speeded up by the factor $(8f)/\pi$ proportional to the cavity finesse. All happens, indeed, as if the atoms were not radiating alone, but interacting with $(8f)/\pi$ successive images in the cavity walls. As far as the emission process is concerned, one can thus replace the N_0 atoms in the cavity by $(8f/\pi)N_0$ atoms in free space distributed along an effective length $(8f/\pi)L$. The condition (26) for overdamped behavior appears in this context as a condition equivalent to the Arecchi-Courtens limitation to super-radiance in free space.[15] It means that the light propagation time along the effective medium on length $(8fL)/\pi$ has to be shorter than the super-radiant time T_R of the $(8fN_0)/\pi$ fictitious atoms. As Arecchi and Courtens have noted, if this condition is not met, super-radiance breaks into several pulses which correspond, in our transient maser problem, to the oscillatory regime. The solution of the damped pendulum equation (28) with an initial condition $\theta_0(0)=\theta_0^i$ has been given in many publications.[6,7] One finds for the radiated intensity

$$\left[\frac{d\theta_0}{dt}\right]^2=\frac{1}{4T_R^2}\frac{1}{\cosh^2\left[\dfrac{t-t_D}{2T_R}\right]} \tag{30}$$

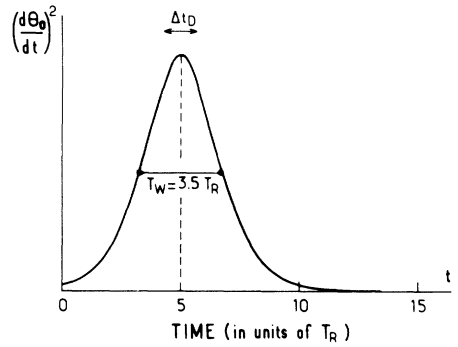

FIG. 6. Hyperbolic-secant solution of the maser evolution equation in case of a small radiating sample. Time is measured in units of T_R. Curve shown corresponds to an initial condition such that $\ln 2(\theta_0^i)^{-1}=5/2$. Arrow indicates the domain of fluctuation of the pulse delay.

with

$$t_D=-2T_R\ln\left[\frac{\theta_0^i}{2}\right] . \tag{31}$$

Equation (30) describes a "hyperbolic-secant" radiation pulse, with a width $T_w\simeq 3.5T_R$ and a maximum occurring after a delay t_D (see Fig. 6). This delay depends, through Eq. (31) upon the choice of initial condition θ_0^i. The statistics of pulse to pulse delay fluctuations can thus be obtained by combining Eq. (21) and (31) with $\bar{\theta}$ being given by Eq. (22) or (23). After a straightforward derivation,[7] one finds the probability law $P(t_D)$ of finding a delay t_D:

$$P(t_D)=\frac{N_0(T)e^{-t_D/T_R}}{T_R}\times\exp[-N_0(T)e^{-t_D/T_R}] , \tag{32}$$

the average delay being

$$\langle t_D\rangle=T_R\ln N_0(T)=T_R\ln\left[\frac{N_0}{1+\bar{n}_B}\right] \tag{33}$$

and the variance of the delay distribution being[7]

$$\Delta t_D=(\langle t_D^2\rangle-\langle t_D\rangle^2)^{1/2}=1.3T_R . \tag{34}$$

These results, presented here in the general case of blackbody radiation triggering, are mere generalization of results derived in Ref. 11 in the case of $T=0$ spontaneous emission initiation of super-radiance $[N_0(T)=N_0]$. This generalization is of course based on the assumption that the statistics of initial

conditions remain Gaussian when the triggering is due to blackbody photons, a result stated without demonstration in Sec. II E, and one that we will discuss in more details in the next paper of this series.

H. Damped regime in the large active volume case: Limited super-radiance

In the case of large active samples, the pulse profile [solution of Eq. (29)] can no longer be expressed in a simple analytical form. Its shape and general features remain similar to the small sample case solution, with some simple modifications. First, there is a lengthening of the emission time scale, coming from the fact that the atom-field coupling is, on the average, reduced by a factor two. In the linear regime (small θ_0), the characteristic evolution time of θ_0 changes from $2T_R$ in the small case (where $\sin\theta_0$ is equivalent to θ_0) to $4T_R$ in the large sample case [where $J_1(\theta_0)$ is equivalent to $\theta_0/2$]. As a result, the emission delay t_D is multiplied by a factor of the order of two. This change in emission delay is correlated to a change in the total amount of radiated energy per pulse. For the same number of atoms N_0, there is always less energy radiated in the large active sample case than in the same sample case. This is clearly related to the fact that the final state reached by the atomic system is different in both cases. For a small radiating volume, the equilibrium state of the pendulum is reached for

$$\theta_0^{\text{equ}}=\pi \tag{35}$$

and the atoms go all the way down to their lower state [$n_a(\pi)=\cos\pi=-1$ according to Eq. (18)]. For a large emitting volume, on the other hand, the final state corresponds to the first minimum of $J_0(\theta_0)$ reached for

$$\theta_0^{\text{equ}}=3.83 \tag{36}$$

which, according to Eq. (19) corresponds to

$$n_a(\theta_0^{\text{equ}})=J_0(3.83)=-0.2\ .$$

This means that about 30% of the atoms remain in the excited state after the emission has ended and, thus, less energy has been emitted in the field. The atomic polarization left in plane z after the emission is according to Eq. (12b)

$$\mathscr{P}(z,t=\infty)=\frac{i}{z_1-z_2}N_0 d e^{i\phi}\sin(3.83\cos kz)\ . \tag{37}$$

There is thus a macroscopic atomic polarization remaining at each point of the active medium. However, $\mathscr{P}(z,t=\infty)$ has opposite phases at various points along the z axis, since the argument of the sine in Eq. (37) is alternatively smaller or larger than π. It appears that the emission from the medium is inhibited because, for the particular value $\theta_0=3.83$, the various planes of dipoles interfere destructively. One has, indeed, according to Eqs. (16) and (19)

$$\begin{aligned}\int_{z_1}^{z_2}\mathscr{P}(z,t=\infty)\cos kz\,dz&=\frac{i}{z_1-z_2}N_0 d e^{i\phi}\int_{z_1}^{z_2}\sin(3.83\cos kz)\cos kz\,dz\\&=-iN_0 d e^{i\phi}\frac{dn_a}{d\theta_0}(\theta_0=3.83)\\&=+iN_0 d e^{i\phi}J_1(3.83)=0\ .\end{aligned} \tag{38}$$

In other words, the limitation to the super-radiant emission is due to a dephasing of the dipoles belonging to different planes. This dephasing is precisely such that there is a net cancellation of the field radiated in the cavity. This effect is quite different from the end of the emission in the small sample case, where the radiation process stops because all the dipoles simultaneously vanish. For large active media, the dipole dephasing occurs because they are unevenly coupled to the field. Those which are at antinode positions evolve faster than those close to the nodes. The evolution stops when, as a result of this dephasing, the system reaches the state described by formula (37). This peculiar situation, in which nonvanishing atomic dipoles cannot radiate any longer because of destructive interference, has been already discussed in the context of various theoretical super-radiance studies.[7,16] It has been given the name of "subradiance" or limited super-radiance.

I. Evaluation of Rydberg maser thresholds

We have so far neglected the various relaxation effects responsible for the damping of the atomic polarization in the maser cavity. This approxima-

tion is justified only far above threshold, where the radiative coupling of the atoms with the cavity mode largely overcomes relaxation. Near threshold, these damping processes are, however, in strong competition with maser action and have to be taken into account in order to study the conditions for the oscillation to occur. Among potentially important damping effects, one should consider (i) the total radiation decay of the Rydberg levels involved in the transition towards other states. This involves spontaneous emission and blackbody radiation induced effects as well. (ii) Collision processes between Rydberg atoms and background gas or Rydberg-Rydberg collisions. (iii) Stark dephasing due to spurious electric fields acting on these very polarizable atoms, and, at last, (iv) velocity dependent effects such as Doppler shifts and limitations due to finite transit time of atoms across the cavity mode. A careful study[17] of the broadening of Rydberg transitions in cavity similar to the one used in this work has shown that the velocity dependent effects are, for low density samples, at least, the dominant damping mechanisms. [Processess (i) and (iii) quoted above contribute, indeed at most, to a few kHz to the linewidth of the maser transition. Collisions with background gas are negligible. Rydberg-Rydberg processes[18] do not enter into play at densities below 10^9-10^{10} cm^{-3}, and are negligible for active samples with about 10^4-10^5 atoms in a volume of the order of 1 mm^3 or more.]

In our maser, the atoms are propagating along a direction perpendicular to the cavity axis (see Fig. 1). This configuration makes the Doppler effect in the cavity negligible (residual transverse velocity of the order of 10 m/s) so that the threshold is essentially due to transit time limitation. The transit time through the cavity waist is

$$T_t^* = \frac{w_0/\sqrt{2}}{\bar{v}} \tag{39}$$

[where $\bar{v}=1.88\ (k_B T/m)$ is the beam average velocity, and $w_0/\sqrt{2}$ the radius of the photon storage active region]. With $\bar{v}\sim 890$ m/s, and $w_0\sim 1$ cm, one gets, typically, $T_t^*\sim 10^{-5}$ s.

A qualitative estimate of the threshold is obviously obtained by equaling the unperturbed average delay t_D to T_t^*. In fact, a more quantitative description, taking into account the actual motion of each atomic velocity group through the field mode, confirms within a few percent these intuitive results:

$$T_R \ln\left[\frac{N_0}{1+\bar{n}_B}\right] \lesssim T_t^* \ . \tag{40}$$

Taking into account Eqs. (25), (3), (5), and (39), this condition can also be expressed as a minimum requirement for the number of inverted atoms:

$$\frac{N_0}{\ln\{N_0/[1+(\bar{n}_B)]\}} \gtrsim 2.5\times 10^{-46}\frac{\bar{v}w_0\lambda}{fd^2} \ , \tag{41}$$

where $\bar{v}$, w_0, λ, and d^2 are expressed in MKSA units. This relation nonsurprisingly shows that the atom number threshold is inversely proportional to the cavity finesse and to the square of the electric dipole matrix element d. In Rydberg atoms with $n\sim 30$, this parameter d is currently three orders of magnitude larger than in ordinary angstrom-size atoms or molecules. As a result, the Rydberg-atom thresholds given by Eq. (41) (a few thousand atoms for an $f\sim 100$ finesse; see Sec. V) are six to seven orders of magnitude smaller than for ordinary masers operating in similar cavities at comparable wavelengths.

Note that the present discussion implicitly assumes that the number $(k_B T)/(\hbar\omega)$ of blackbody photons stored in the cavity is much smaller than the number of active atoms, so that the effect of the thermal field at time $t=0$ can be described as a small tipping angle $\bar{\theta}(T)\ll 1$ [see Eq. (23)]. This requires, in particular, that the logarithm in Eq. (41) should be large compared to one, i.e.,

$$N_0 \gg \bar{n}_B \ . \tag{42}$$

J. Polarization of the Rydberg-maser radiation, simple case of an $nS_{1/2}\rightarrow n'P_{1/2}$ transition

Let us now briefly discuss the polarization properties of the maser emission in the simple case of an $nS_{1/2}\rightarrow n'P_{1/2}$ transition. As we have shown in Sec. II A, this case can be analyzed in terms of a superposition of two independent two-level atom systems (see Fig. 2). If the pumping process is performed with unpolarized light (more precisely with light having no circular polarization), the two

$$|nS_{1/2},m_J=-\tfrac{1}{2}\rangle$$

and

$$|nS_{1/2},m_J=+\tfrac{1}{2}\rangle$$

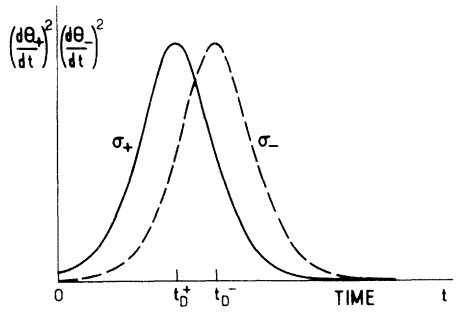

FIG. 7. Example of time variation of the two σ_+ and σ_- components in the maser emission ($nS_{1/2} \rightarrow n'P_{1/2}$ transition). Two delays t_D^+ and t_D^- are slightly shifted with respect to each other by a random amount. In this case the resulting field starts as a σ_+ field, then becomes elliptically polarized [exact linear polarization at time $t=(t_D^+ + t_D^-)/2$] and ends up as a σ_- field. During the bulk of the pulse emission the field polarization is nearly linear.

sublevels are equally populated at time $t=0$. The σ_+ and σ_- field components are then emitted with equal amplitudes in the maser cavity. However, the initial quantum fluctuations are obviously uncorrelated for the two field components. This means that for each realization of the experiment, there is a random phase and delay difference between the σ_+ and σ_- components. The phase difference $\phi_+ - \phi_-$ is completely random. The average value of the pulse delay difference $t_D^+ - t_D^-$ is of the order of $1.3T_R$ [see Eq. (34)], i.e., only about one third of the width of each pulse. As a result, the total field radiated in the cavity is the sum of two slightly time shifted σ_+ and σ_- bell-shaped pulses with random phases (see Fig. 7). The resulting field has a time-varying polarization. It starts with the circular polarization of the component which has been triggered by the large fluctuation and ends with the other circular polarization. For most of the field emission, however, the two components have comparable amplitudes and the field polarization is elliptical or linear. Near the emission maximum, the σ_+ and σ_- amplitudes are nearly equal and the polarization is practically linear, with a direction defined by $\phi_+ - \phi_-$. These polarization features randomly change from one realization of the experiment to the next, with a statistics which can be entirely deduced from Eqs. (20) and (21). The most important feature is that the polarization of each pulse is nearly linear at the time of maximum emission, with a polarization rotating randomly from one pulse to the next. If the field is coupled outside the cavity through a rectangular waveguide acting as a linear polarizer, the maximum peak intensity radiated into this waveguide will exhibit 100% pulse to pulse fluctuations reflecting the random pulse to pulse rotation of the maser polarization.

We have restricted here the description of the maser polarization to a simple case corresponding to a situation realized in our experiments. It is clear that other pumping schemes or level structures could lead to different predictions. More general discussions of polarization effects in super-radiance can be found in Refs. 7 and 8.

K. Discussion of the two-level approximation validity. Qualitative analysis of multilevel effects in Rydberg-maser emission

Let us now discuss the validity condition of the two-level atom approximation made throughout this section. The maser emission on the transition selected by the resonant cavity is, in fact, in competition with super-radiant (mirrorless) emission on other transitions originating from the same initial level. Let us consider one of these potentially competing transitions and let us call ω' its frequency and Γ' its partial radiative decay rate. The super-radiant emission on this transition would occur in a direction depending on the actual geometry of the active medium and not on the cavity geometry, with a diffraction solid angle μ'. The corresponding characteristic emission time on this transition is $T'_R = \Gamma' \mu' N_0$. The condition for this super-radiant effect to be quenched by the maser emission on the cavity selected frequency is simply

$$T_R < T'_R \ , \tag{43}$$

or else

$$f > \frac{\Gamma'}{\Gamma} \frac{\mu'}{\mu} \ . \tag{44}$$

In other words, the cavity finesse should be larger than the product of the branching ratio of the corresponding transitions by the ratio of their emission solid angles. With cavity finesses as large as a few hundred, such a condition is easy to meet. Owing to the nonlinear character of the emission process, the super-radiant emissions on the cavity nonselected transitions are then totally suppressed and the two-level atom approximation is justified. This is true, however, only when the cavity is precisely tuned to the frequency ω. If the $\Gamma'\mu'$ product relative to the transition at ω' is larger than $\Gamma\mu$, super-radiance on this transition will take over and quench the maser emission as soon as the cavity

will be detuned to a frequency $\omega+\delta\omega$ such that its effective finesse is reduced by the ratio $\Gamma'\mu'/\Gamma\mu$. The transition from one regime to the other is very sharp, due to the nonlinearity of the coupled atom-fields system. Hence, one expects to observe sudden changes in the system emission behavior when the cavity eigenfrequency is swept around ω. The atomic emission should suddenly shift from ω' to ω and then back from ω to ω' (we disregard here frequency pulling effects which, on top of this gross effect, should also slightly shift the maser frequency around ω). This competing effect results in a dramatic change of the Rydberg level populations with cavity tuning as will be described in details in Sec. V.

III. DESCRIPTION OF THE RYDBERG-MASER SETUP

In this section, we describe, in detail, the experimental apparatus on which the Rydberg-maser action has been obtained and we discuss some orders of magnitude relevant to the operation of these devices. As explained in Sec. I, evidence of the maser action has been obtained either by direct detection of the maser radiation[4] or indirectly, by state population analysis.[2] Only the first method permits a real time analysis of the pulse shapes, fluctuations, and delays. However, since it requires a local oscillator and a high quality mixer, it is not versatile and cannot easily be extended to the whole range of maser frequencies (in particular, in the submillimeter domain). The second method offers the valuable advantages of higher sensitivity (emission of only a few atoms can be detected) and simplicity of operation. All masing transitions can be observed without modification of the apparatus. However, since it is destructive for the atomic polarization, this method gives information on the system evolution at a single time only. By sampling a large number of pulses detected with variable delays, the evolution of the system can be studied by this method. We have, indeed, performed such a sampling analysis in the case of mirrorless superradiance, where the field ionizing plates could be placed around the active medium.[2] For Rydberg masers, the emission occurs in a rather small cavity and it is impossible to have field plates near the sample, where they would perturb the cavity mode pattern and hence the field evolution. The plates are thus placed downstream the atomic beam (see Fig. 1) and the detection occurs only after the atoms have left the cavity, thus yielding only the final state of the maser evolution [i.e., $\theta_0(+\infty)=\theta_0^{\text{equ}}$]. This very simple information already provides a lot of interesting features of the Rydberg masers; it allows us to identify without ambiguity all the transitions on which the masing action is observed, to estimate accurately the maser thresholds, to put in evidence size sample effects (π pulse versus limited super-radiance) and to study various competing effects between maser action and mirrorless superradiance on other transitions sharing the same upper level. In this paper, we restrict ourselves to the detailed description of the indirect detection procedure, we analyze all the information it provides about the maser emission and compare it with the theoretical predictions of Sec. II. The direct detection method will be described in detail in the next paper.

A. Atomic beam and excitation of Rydberg atoms

The general features of the maser apparatus have been briefly described in Sec. I and the sketch of the apparatus is given in Fig. 1. We give, in this section, more details about the atomic beam and the Rydberg excitation process.

The beam of Na atoms, originating from an oven heated at about 400 °C has, when it crosses the cavity, a diameter of about 0.5 cm (this dimension is controlled by a diaphragm). The atom density is of the order of 10^{11} cm^{-3} and the beam divergence is about 5°. The atoms are excited in the upper Rydberg level of the maser transition by two collinear N_2 laser pumped pulsed dye lasers crossing the atomic beam at right angle inside the cavity. The lasers are tuned, respectively, to the $3S\rightarrow 3P_{1/2}$ ($\lambda_1=5896$ Å) and $3P_{1/2}\rightarrow nS_{1/2}$ transition ($n\sim 20$ to 40; $\lambda_2\sim 4100$ Å). The laser pulse lasts about 5 ns. The blue laser is amplified to about 10-kW peak power by an amplifying dye cell pumped by the same N_2 laser. This power is large enough to create more than 10^6 Rydberg atoms at the intersection of the atomic and laser beams (for $n\sim 20$ to 40). The size of the active volume in the cavity is controlled by adjusting the focus of the pumping laser beams with lenses of various focal lengths. This focus can be reduced to a spot less than 0.2 mm in diameter (i.e., much less than λ) or expanded over half a cm (i.e., much more than λ), thus allowing us to check the sample size effects discussed in subsection II H. During the ~ 1 μs maser emission duration, it is justified to neglect the transverse atomic beam diffusion along the cavity axis. In fact, the shape of the active medium is a small cylinder whose axis is

perpendicular to the cavity one and whose length ($\sim$0.5 cm) is smaller than the cavity waist. Hence, the theoretical model of Sec. II B (atomic slab comprised between two abscissas z_1 and z_2) is a fair approximation of the actual experimental situation.

B. Maser cavity

The atoms thus prepared at time $t=0$ couple to the cavity and emit a radiation burst. The choice of an open Fabry-Perot structure for the cavity is very convenient for various reasons. The semiconfocal structure (one spherical mirror and one plane mirror at a distance equal to the focal length of the spherical mirror) gives a large transverse access. It is also well suited for microwave irradiation since it permits to reduce to negligible amounts the diffraction losses with mirrors having transverse sizes of about only 10λ. Moreover, this structure is very convenient for cavity tuning; one mirror is mounted on a screw drive insuring a smooth translation along the cavity axis resulting in a continuous change of the cavity length around its nominal value.[19] Since the parallelism of the mirrors is not critical in this configuration, this tuning procedure is not detrimental to the quality factor of the cavity.

Two cavities (sketched on Fig. 8) have been used in turn for different emission wavelengths. The first one [Fig. 8(a)], optimized for a 60–90-GHz band, has a length L of 72 mm (spherical mirror radius $r=2L=144$ mm). The diameters of the spherical and plane mirrors are 50 and 35 mm, respectively. The Q factor of the cavity, made of brass, is about 6250 at 108 GHz, corresponding to a finesse $f=120$. The waist of the Gaussian mode of the field is $w_0=8$ mm. The microwave is coupled in and out the cavity through small holes (diameter 1.3 mm) drilled at the center of the mirrors. The plane mirror is connected to a circular waveguide which does not polarize the microwave. The spherical mirror is coupled to a rectangular guide carrying the signal to a mm-wave detector (Schottky diode receiver described in next paper). The second cavity [Fig. 8(b)], smaller in size, is optimized for higher frequencies (200–300 GHz). It has a focal length of 51 mm ($r=2L=102$ mm is the radius of the spherical mirror). The mode waist is $w_0=4$ mm at $\lambda=1$ mm, and the mirror diameter is 25 mm. The quality factor, $Q=30\,000$ at 300 GHz, corresponds to a finesse $f=300$. Only one mirror is drilled in this cavity which is not designed for direct coupling to a mm-wave receiver. Both cavities are operating in highly excited modes in all our masers ($L=q\lambda/2$ with $q\sim 50$ to 100).

The discussion of Sec. II has shown that the two important cavity parameters relevant to the maser emission are its damping time T_{cav} and its diffraction angle

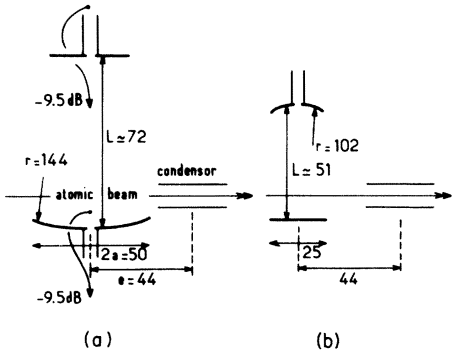

FIG. 8. Two Fabry-Perot semiconfocal millimeter cavities used in our experiments. Distance L between mirrors can be adjusted around the focal length$=r/2$ in order to tune the cavity on the chosen wavelength λ, according to the formula $8L/\lambda=4q+1$, where the integer q is the number of half wavelengths of the standing wave (longitudinal mode). Mirror's diameter $2a$ is chosen not too large ($a^2/r\lambda\simeq 1$) in order to reduce the transverse modes without attenuating the longitudinal mode. Because of the finite lifetime of the atoms, one detects only a fraction of them after their flight of length e between the center of the cavity and the center of the condenser (lengths on figure are in mm).

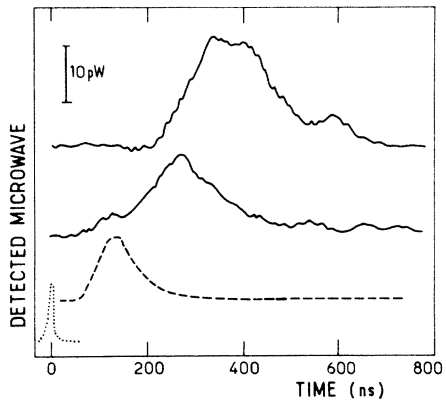

FIG. 9. Two typical maser pulses detected at 107 892 GHz ($33S\rightarrow 32P_{1/2}$ transition in Na). Dotted curve around time $t=0$ represents the pumping laser pulse. Dashed curve is the percussional response of the microwave receiver. Upper trace is a 20 pW microwave burst, corresponding to an actual $\sim$200 pW emission by the atoms [taking into account the 9.5 dB output coupling cavity loss, see (1) in Fig. 8]. The estimated number of atoms is $\sim 5\times 10^5$.

$$\mu=\frac{3}{4\pi^2}\frac{\lambda^2}{w_0^2}\,.$$

Let us briefly estimate here the order of magnitude of these quantities, whose precise value depends, of course, upon the cavity and its operation frequency. The damping time $T_{cav}=fL/\pi c$ is typically of the order of 10 ns. It can be inferred from the measured values of the f and L parameters or, which is equivalent, from the measure of the width $\Delta\nu=(2\pi T_{cav})^{-1}$ of the cavity resonance which is typically of the order of 17 MHz. As for the μ parameters, they are of the order of 10^{-2}.

C. Detection of maser emission

Figure 9 shows a typical example of microwave maser bursts detected by the Schottky heterodyne receiver.[4] As explained above, we do not describe in this paper this detection procedure. We show this recording here only for sake for completeness, to give the reader an idea about the signal time dependence, which is not directly accessible to the indirect detection method we focus on in this paper. This method, as we have seen, consists in analyzing the state of the atoms after they have left the cavity. Owing to their long natural lifetimes (20 to 50 μs), 10 to 30% of the atoms can indeed survive over a length of 4.4 cm downstream. It is then possible to analyze their quantum states by sending them through parallel electric field plates (Fig. 1). The principle of the analyzing method has been described in Ref. 20. It is recalled on Fig. 10 which sketches the time variation of the electric field generated by the plates and the electron peak signals produced by this field. A ramp of electric field $F(t)$ raising in a time of the order of 1 μs is applied to the atoms. $F(t)$ starts a delay $t_0\sim 30$ μs after the laser excitation, which leaves the atoms time to reach the detection region. The time varying field $F(t)$ reaches at different times t_i,t_f the threshold field F_i,F_f for ionization of successive Rydberg levels. Roughly speaking, the more bound the Rydberg state is, the higher is the field needed to break the atom. This produces time-resolved electron pulses which are detected with the help of a high gain electron multiplier (E.M. on Fig. 1). (The produced electrons cross the field plates through a grid before reaching the E.M.)

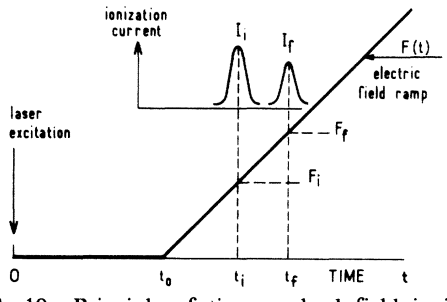

FIG. 10. Principle of time-resolved field ionization detection of the maser emission. The maser action occurs between times $t=0$ and t_0. Then the electric field ramp is applied. Atoms in level i, which ionize in field F_i, give rise to an electron peak I_i at time t_i. Atoms in the more bound level f give rise to a later peak I_f at time t_f. The maser transition $i\rightarrow f$ results in a change of the respective amplitudes of peaks I_i and I_f.

The timing of the electron pulses in the electric field ramp allows us to analyze the population of the Rydberg states at the time the atoms have left the cavity (it is justified to assume that the atom evolution is negligible between this time and the onset t_0 of the electric field ramp). The detailed time dependence of the electron pulses is clearly very difficult to predict theoretically. It varies with the electric field slew rate[21] and depends upon the complex variation of the Stark energy diagram of the Rydberg atom in the time-varying electric field. The only important feature of this electron peak for our experiment is, however, the fact that its shape and delay depend upon the quantum state of the

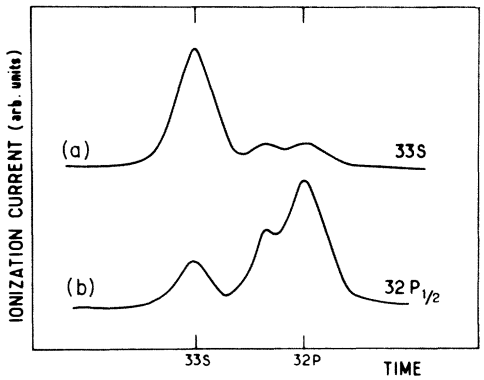

FIG. 11. Examples of time-resolved ion signal (averaged over 100 laser pulses). Trace (a) is the ion signal associated to field ionization of the 33S level, directly prepared by laser excitation. Trace (b) is the ion signal corresponding to the $32P_{1/2}$ level. This level is prepared by laser excitation of the 32S level (which ionizes in a field larger than the one applied to the atom) followed by a microwave-induced $32S\rightarrow 32P_{1/2}$ transition. The 33S and 32P markers on the time axis indicate the respective maxima of these ion pulses. Note the partial time overlapping of these two signals.

Rydberg atom at the time the field is applied. These features are reproducible from one realization of the experiment to the next for a given electric field ramp.

Figures 11(a) and 11(b) show, as an example, the electron peak "signatures" for levels $33S_{1/2}$ and $32P_{1/2}$, the atoms being directly excited inside the field plate detector. One clearly notices that the two electron peaks have different shapes, with an ionization field on the average larger (i.e., a longer delay) for the more bound $32P_{1/2}$ state. (Note also the complex multiple peak structure of these electron signals and the fact that a precursor peak in the $32P_{1/2}$ signal overlaps with the main component of the $33S$ signal.)

These signals are used to detect the maser emission in the following way: In a first stage, the cavity is mistuned off resonance and the atoms are excited inside it in a given Rydberg level (for example, $33S_{1/2}$). One checks that the electron peak signature does indeed correspond to that level. One then tunes the cavity on resonance with the transition to be studied (for example, the $33S \rightarrow 32P_{1/2}$ one) and detects in the electron peak signal the appearance of a contribution coming from the lower level of the transition. This yields the proof that the cavity-induced maser transition has occurred. The method obviously applies without modification to a very large range of maser transition frequencies.

This method is also very convenient in order to calibrate the absolute number of active Rydberg atoms in the system. The time integral of the electron peak signal is indeed proportional to the number of produced ions and hence to the initial Rydberg-atom population (since all atoms are ionized and collected). The proportionality constant depends upon the E.M. gain, which is calibrated in the following way: Through the use of the precalibrated optical filters, the laser beams are attenuated to a level such that electron counting becomes possible. The number of electron counts gives the number of atoms excited at the low light pumping level. Knowing the filters attenuation factor, and assuming that the pumping light is never saturating the atoms, the absolute number of atoms excited under strong pumping irradiation can be inferred. This number has yet to be corrected by multiplying it with a factor larger than one, accounting for Rydberg atom losses between the cavity and the detector. These losses are due to atomic beam lateral diffusion, to Rydberg-atom spontaneous decay, to transfers induced by blackbody radiation during the time of flight between the cavity and the detector. The loss factor, of the order of 10 in our experiments, is measured by comparing the electron signals obtained when the atoms are excited in the cavity with the ones which are got when the laser beams are directly sent into the field detection plates. This whole counting procedure allows us to evaluate the number of atoms taking part in the maser emission with an uncertainty that we estimate to about $\pm 30\%$. Typical numbers N_0 of atoms in our masers are measured to be in the range $10^5 - 10^6$, although we will see that atom numbers as low as 10^4 have been found near threshold.

D. Operating regime of the Rydberg masers

The above discussion allows us to compare the orders of magnitude of the cavity damping times $T_{\rm cav}$ and of the expected characteristic emission times T_R and to reach a conclusion concerning the operating regime of the Rydberg masers. With typical values $\Gamma = 10^2\ \mathrm{s}^{-1}$, $\mu = 10^{-2}$, $N_0 = 10^5$, and $f = 100$, one finds, according to Eq. (25), $T_R = 100$ ns. This corresponds to characteristic emission delays

$$\bar{t}_D = T_R \ln N_0(T)$$

of the order of 400 ns, in quite good agreement with typical experimental results (see, for example, the time scale on Fig. 9). Comparison of T_R with $T_{\rm cav}$ leads to the conclusion that the masers operate in the overdamped regime, where the field in the cavity can adiabatically follow the atomic polarization. No oscillation ringings are expected in this case. This justifies that we have focused the discussion of Sec. II on that regime. It should be noted, however, that a moderate increase of the cavity quality factor, which would increase $T_{\rm cav}$ and at the same time decrease T_R for the same number of atoms, would bring the masers in the oscillatory regime of operation. We discuss the possibility of achieving this condition in a special case at the end of this paper.

IV. DETAILED STUDY OF THE $33S \rightarrow 32P_{1/2}$ MASER EMISSION IN Na

As a first example of Rydberg-maser emission, we now analyze in detail the various experimental checks of the theory we have made on the $33S \rightarrow 32P_{1/2}$ transition in Na, around 108 GHz using the large cavity. [See Fig. 8(a).]

Figure 12(b) shows a typical transfer signal to the $32P_{1/2}$ final state of the transition when the cavity

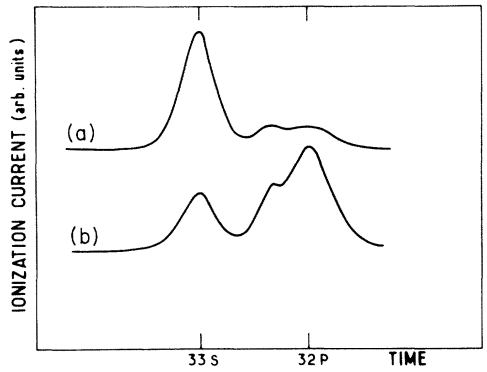

FIG. 12. Field ionization detection of maser action on the $33S \rightarrow 32P_{1/2}$ transition. (a) Off-resonant cavity: One observes the signal of the initially prepared $33S$ level similar to trace (a) of Fig. 11. (b) Resonant cavity and small size sample medium centered at a maximum field position of the standing wave: One observes a signal very similar to trace (b) of Fig. 11 characteristics of the $32P_{1/2}$ level alone. The maser emission is practically a π pulse ("total super-radiance").

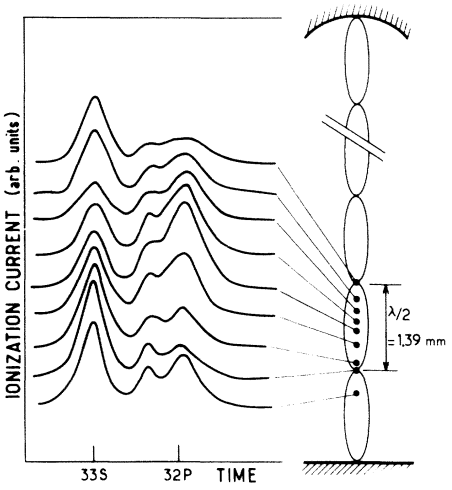

FIG. 13. Periodic variation of the time-resolved field-ionization signal when the small size active medium is displaced along the longitudinal cavity mode. Each trace corresponds to a different position indicated on the right part of the figure.

is tuned to the resonant frequency at 107 892 GHz. Figure 12(a) gives for comparison the corresponding signal when the cavity is off resonant. A similar transfer signal is obtained for a cavity tuning to the nearby the $33S \rightarrow 32P_{3/2}$ transition associated to the other fine-structure component in the final state (at 107 714 GHz). Measurement of the cavity length changes when going from one line to the other allows us a determination of the fine-structure interval.[2,3]

For the recording in Fig. 12, the active medium was focused in a 0.2-mm spot at a maximum electric field position in the cavity. By comparing the ion peak signal in Fig. 12(b) to the one in Fig. 11(b), corresponding to a direct excitation of the $32P_{1/2}$ level, one checks that the maser emission completely depletes, in this case, the upper level of the transition (π pulse super-radiance). When the active medium is defocused and is made much larger than the emission wavelength, only a partial transfer to the lower level is observed, with an ion peak signal exhibiting a mixture of $33S_{1/2}$ and $32P_{1/2}$ level population. We thus qualitatively check the predictions of Sec. II H.

Coming back to the case of a small active medium (focused excitation), we have, in another experiment, scanned the active medium position along the axis of the cavity, while keeping the other excitation conditions constant (same number of excited atoms). We have analyzed for each position the final state of the maser transition. We have checked in this way the coskz dependence of the atom-field coupling. When going away from an antinode position, coskz decreases and the atomic polarization evolution slows down because the atom-field coupling becomes smaller. The fraction of atoms transferred to the lower level of the transition at the moment the atoms leave the cavity decreases. At some point, close to the node position, practically no atoms are transferred any longer (maser under threshold). The transfer resumes again when coskz increases towards the next electric field maximum value. Figure 13 exhibits clearly the corresponding periodic variation of the maser output. In this experiment, the masing Rydberg atoms can be viewed as a sensitive probe allowing us to explore the mode structure of the millimeter-wave cavity.

V. DESCRIPTION OF THE WHOLE SERIES OF OBSERVED MASER TRANSITIONS. COMPETITION WITH SUPER-RADIANCE AND CASCADE EFFECTS

Signals similar to the ones described in Sec. IV have been observed on a wide range of millimeter-wave transitions in Na. Figure 14 shows a section of the Rydberg level energy diagram with the detected maser transition represented by arrows. Series of

$$nS \rightarrow (n-1)P_{1/2,3/2} \quad (\Delta n = 1)$$

and

$$nS \rightarrow (n-2)P_{1/2,3/2} \quad (\Delta n = 2)$$

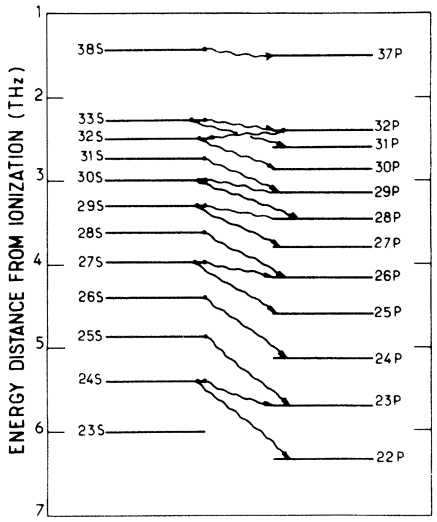

FIG. 14. Energy diagram of Na Rydberg states exhibiting the $\Delta n=1$ and 2 maser transitions observed in this work in the frequency range 69 to 947 GHz. Each transition is split into two fine-structure components $nS\rightarrow n'P_{1/2}$ and $nS\rightarrow n'P_{3/2}$. From the tuning positions of the cavity, one can deduce the resonance frequencies with a relative accuracy of the order of 10^{-4}.

lines have been observed with n as high as 38 for $\Delta n=1$ and n as low as 24 for $\Delta n=2$ transitions. The detected maser frequencies thus cover a wide interval ranging from $\nu'_M=69.1$ GHz ($38S\rightarrow 37P_{3/2}$ line) up to $\nu''_M=946.8$ GHz ($24S\rightarrow 22P$ line). The corresponding wavelengths are $\lambda'_M=4.34$ mm and $\lambda''_M=317$ μm. The shortest wavelengths transitions in this series could already be considered as far infrared laser transitions. Extension of this frequency spectrum towards the microwaves or towards the infrared presents no difficulty and is just a matter of cavity tuning and laser-pumping frequency adjustments.

At this point, let us describe how we have unambiguously assigned the various maser transitions. The upper nS level is, of course, known from the pumping-laser wavelength. The complete assignment of the maser transition thus consists in identifying the lower level $n'P$, which is performed as follows.

(i) The frequency $\nu_{nS\rightarrow n'P}$ of the transition is determined by cavity tuning. The distance L between the mirrors of the Fabry-Perot semicofocal cavity is measured within a few micrometers. It yields a series of possible resonance frequency $\nu_{q,m,m'}$ defined with a typical relative accuracy $\Delta\nu/\nu=10^{-4}$:

$$\nu_{q,m,m'}=\left[\frac{c}{8L}\right](4q+1+m+m') .$$

q is an integer labeling the principal mode. m and m' are integers which, when different from zero, label transverse modes, generally much more attenuated than the principal mode. One compares the series of $\nu_{q,m,m'}$ values corresponding to the measured length L with the series of $\nu_{nS\rightarrow n'P}$ transition frequencies known from previous spectroscopy studies in sodium.[22] This procedure unambiguously determines q,m,m' and, hence, the final state $n'P$ of the transition. This assignment can be checked by changing L by $\pm\lambda/2$ (so that q is changed into $q\pm1$), the maser being again observable at this new cavity tuning.

(ii) The lower level assignment can also be made by mere inspection of the field ionization peak delay and shape. This procedure might sometimes be ambiguous since close levels ionize in approximately the same fields and the signals overlap in time (in particular, fine-structure $nP_{1/2}$ and $nP_{3/2}$ states, belonging to the same electronic level, cannot be distinguished easily).

(iii) In order to remove this ambiguity, one can also apply a small millimeter-wave field tuned to a known transition connecting the assumed lower level of the transition to a third Rydberg state. Although the maser cavity is not in resonance with this field, the transition can be, nevertheless, easily induced since it requires only tiny amounts of microwave. If this field saturates the corresponding transition, it prevents the atomic dipoles to build up on the maser transition sharing a common level and quenches the maser signal, thus unambiguously assigning the lower level of the maser emission.

Using tests (i), (ii), and sometimes (iii), we have been able to assign precisely all the lines shown on Fig. 14.

Since $\Delta n=1$ and $\Delta n=2$ maser lines share the same upper level and, since they have very different thresholds (see Sec. VI), there may be strong competing effects between maser action on one line and free super-radiance on the other. These effects illustrate the qualitative theoretical predictions made in Sec. II K. Figure 15 shows, as an example, the maser signals one can observe after excitation of the $27S$ level (the number of excited atoms is about 5×10^5 in each trace). On trace (a), the cavity is out of resonance for both transitions and a small transfer towards the $26P$ level is nevertheless observed. This transfer is obviously due to superradiance (threshold for mirrorless emission on a $\Delta n=1$

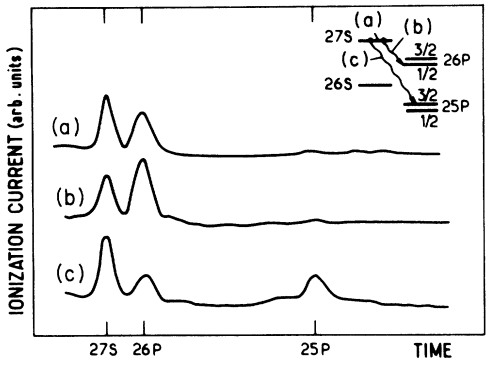

FIG. 15. Competing effects between $\Delta n=1$ and $\Delta n=2$ transitions after excitation of $27S$ level in Na. (a) Cavity out of resonance: One observes a mirrorless super-radiant transfer towards $26P$ level. (b) Cavity on resonance with $27S\rightarrow 26P_{1/2}$ transition: The maser emission on this transition is enhanced (wavelength $\lambda=1.4705$ mm). (c) Cavity tuned on resonance with $27S\rightarrow 25P_{3/2}$ transition: $27S\rightarrow 26P$ super-radiance is quenched and the electron peak corresponding to the $27S\rightarrow 25P_{3/2}$ emission at $\lambda=0.4655$ mm appears (the insert shows the relevant energy levels and transitions).

transition is about 2×10^5 atoms^2). When the cavity is tuned on resonance with the

$$27S\rightarrow 26P_{1/2} \quad (\Delta n=1)$$

line, one observes a strong increase of this transfer, due to the cavity enhancement effect on the medium [trace (b)]. If, on the contrary, the cavity is tuned on the $\Delta n=2$ transition ($27S\rightarrow 25P_{3/2}$), the $27S\rightarrow 26P$ emission is quenched and the atomic population is transferred preferentially to the more bound $25P_{3/2}$ level, yielding an ionization peak at a later time [trace (c)]. Unambiguous assignment of this process is made by applying a mm-wave signal resonant with the $25P_{3/2}\rightarrow 25S$ transition. This field quenches the $27S\rightarrow 25P_{3/2}$ maser line as explained above, and restores the super-radiant transfer $27S\rightarrow 26P$ [one observes a signal identical to trace (a)]. Similar competing effects have been observed on the other $\Delta n=1$ and $\Delta n=2$ transitions. Quite generally, the $\Delta n=1$ lines have a much larger gain than the $\Delta n=2$ ones, so that the maser is close to threshold for mirrorless super-radiance on the $\Delta n=1$ transition when the population inversion is barely enough to sustain maser action on the cavity favored $\Delta n=2$ line. Thus, $\Delta n=2$ masers can only be observed when the cavity is well tuned to the corresponding frequency. Any small perturbation (slight cavity mistuning or small mm-wave field coupled to the lower level of the $\Delta n=2$ line) is enough to quench the $\Delta n=2$ line and to restore the $\Delta n=1$ super-radiance.

These competing effects might be complicated by the occurrence of cascading maser emissions on successive $nS\rightarrow(n-1)P$ and $(n-1)P\rightarrow(n-1)S$ transitions, as shown on Fig. 16. Trace (a) exhibits the ionization signals of the initially pumped $33S$ level, with an off-resonant cavity. A small super-radiant transfer to level $32P$ is observed. If the cavity is tuned towards the $33S\rightarrow 32P_{1/2}$ line or $33S\rightarrow 31P_{3/2}$ line, the $\Delta n=1$ and $\Delta n=2$ maser emissions are observed [respectively, traces (b) and (c)] as explained above. If now the cavity is tuned towards the $32P_{1/2}\rightarrow 32S$ transition, one observes the ion peak signal shown in trace (d). At first sight, it looks similar to the trace (c) signal, with a final-state ion peak occurring at the same time. However, this peak has a different shape, showing that the final state reached in traces (c) and (d) are different. An assignment of these states is made by

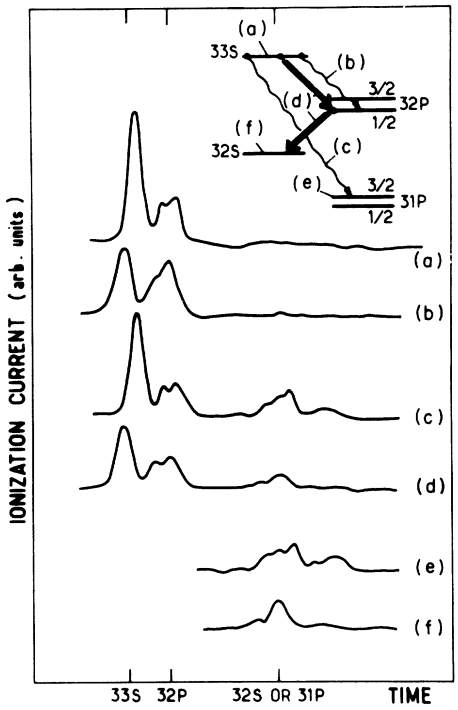

FIG. 16. Cascading maser emission in Rydberg Na states after excitation of level $33S$. (a) Off-resonant cavity: small super-radiant transfer to level $32P$; (b) cavity resonant with $33S\rightarrow 32P_{1/2}$ transition: $\Delta n=1$ maser effect; (c) cavity resonant with $33S\rightarrow 31P_{3/2}$ transition: $\Delta n=2$ maser effect; (d) cavity resonant with $32P_{1/2}\rightarrow 32S$ transition: cascading $33S\rightarrow 32P_{1/2}$ and $32P_{1/2}\rightarrow 32S$ transitions. The first is super-radiant and the second is assisted by the cavity; (e) and (f) signatures of $31P_{3/2}$ and $32S$ levels directly prepared in the field detector. The wavy lines in the energy diagram refer to the direct emission processes (b) and (c). The solid arrows show the cascading emission.

comparing the corresponding electron peaks to the ion peak signatures of directly prepared $31P_{3/2}$ and $32S$ states [traces (e) and (f), respectively]; this test unambiguously shows that the final state in trace (d) is the $32S$ level. The emission process observed in trace (d) seems at first sight peculiar, since it occurs when the cavity is tuned to a transition connecting levels not directly excited by the lasers. The explanation is that we are observing a cascading maser effect; the $33S \rightarrow 32P_{1/2}$ transition occurs first in a super-radiant regime [this emission might also be helped by the fact that the cavity tuned on the $32P_{1/2} \rightarrow 32S$ transition has also a parasitic low-Q mode ($Q \sim 10$) accidentally resonant for the $33S \rightarrow 32P_{1/2}$ line]. After this first emission, a large number of atoms has been transferred to the $32P_{1/2}$ level. The $32P_{1/2} \rightarrow 32S$ maser emission favored by the cavity tuning then occurs, depleting the $32P_{1/2}$ level and populating the final $32S$ state. This explanation is sustained by a very simple mm-wave test. If we apply small mm-wave signal resonant on the $32S \rightarrow 31P$ line, the $32P \rightarrow 32S$ maser emission is quenched and a large population is restored in the $32P$ level [one then observes again the signal of trace (b)].

VI. DETERMINATION OF MASER THRESHOLDS: TOWARDS THE REALIZATION OF "SINGLE-ATOM RYDBERG MASERS"

An important feature of the Rydberg masers in their extremely low threshold of operation, due to the very large electric dipoles associated to the atomic transition (see Sec. II I). This feature is clearly apparent in our experiments. Typical $\Delta n = 1$ maser signals reported above correspond to atom numbers in the range 10^5 to 10^6. Reducing this number by attenuation of the pumping laser beams, we have been able to get maser emission of still smaller atomic systems. We describe in this section these experiments, in which we have measured very low Rydberg-maser thresholds and we discuss the possibility of further improvements which would allow us to realize devices with only a few atoms (ultimately a single atom) coherently interacting with the cavity.

A. Measurement of maser threshold on $\Delta n = 1$ and $\Delta n = 2$ Rydberg transition

In order to check formula (41), we have chosen to determine the threshold of a typical Rydberg maser corresponding to the $33S \rightarrow 32P_{1/2}$ transition ($\lambda_1 = 2.779$ mm; $d_1 = 493$ a.u.). The maser is operating in cavity No. 1 at room temperature ($w_0 = 8$ mm; $f = 120$; $T = 300$ K). We have progressively attenuated the laser beams and tried to detect maser signals corresponding to smaller and smaller atom numbers. For each laser power, we have recorded the field ionization signals and, according to the method described in Sec. III C, deduced the absolute number of excited atoms in the cavity. We have eventually observed a disappearance of the maser transfer for $N_0 = 20\,000(\pm 8000)$ atoms. This number corresponds, in fact, to an inversion twice smaller for each of the two independent transitions

$$| 33S_{1/2}, m_J = \pm \tfrac{1}{2} \rangle \rightarrow | 32P_{1/2}, m_J = \mp \tfrac{1}{2} \rangle \ .$$

The "two-level atom" maser threshold is thus measured to be

$$\frac{N_0}{2} = 10\,000(\pm 4000) \ .$$

On the other hand, formula (41), with $T = 300$ K and $\bar{v} = 890$ m/s, predicts $N_0 = 13\,000$, in agreement with the measured value. Low thresholds of the same order of magnitude have been obtained on other $\Delta n = 1$ Rydberg masers.

We have also measured thresholds of $\Delta n = 2$ maser transitions in cavity No. 2. They have been found typically in the range of 10^5 atoms (for $n \sim 30$). These values are again in fair agreement with theory. The larger threshold values for the $\Delta n = 2$ transitions is partly due to a smaller electric dipole matrix element and partly to a smaller cavity finesse at higher frequencies.

Let us insist once more on the extremely small value of these thresholds, as compared to other masers operating at similar frequencies which usually require at least 10^9 atoms or molecules. The 20 000 atom maser reported above emits a total energy $N_0 \hbar \omega_0$ of 9 eV only. The emission occurring in an average time of the order of 1 μs, the corresponding radiated power is only 10^{-12} W. The fact that such a small amount of radiation is easily detected by the Rydberg-atom field ionization procedure is an indication of the extreme sensitivity of these atoms as detectors of mm waves.

B. Towards masers operating with only a few atoms

The experiments described above clearly indicate that it should be possible to build "maserlike" systems in which the active medium would consist of a few atoms only (ultimately a single one). The threshold for maser operation being, according to

formula (41), inversely proportional to f, an improvement of this parameter should indeed reduce in the same proportion the maser threshold.[23] Of course, when the number of atoms is reduced below a few hundred, it is necessary to reduce also the cavity walls temperature, so that the number of photons radiated by the atoms in the cavity remains larger than the number of blackbody photons [in order to satisfy relation (42)]. Ultimately, one should reduce the blackbody background temperature T to a value such that $k_B T/\hbar\omega \lesssim 1$, i.e, $T \lesssim 5$ K (for $\omega \sim 100$ GHz). Such temperatures can be achieved by cooling the cavity walls to liquid helium (4.2 K). This cooling will also serve another purpose; it will increase the cavity finesse through a reduction of the mirrors resistivity and ultimately should allow us to realize ultra-high Q superconducting cavities with finesse in the 10^5 to 10^6 range.

It is clear that the theory of Sec. II is no longer adequate to describe the evolution of very small atom number masers (the semiclassical point of view adopted there assumes indeed that the number of emitted photons is large compared to one, so that a classical description of the maser field makes sense). In order to study the behavior of these very small masers, one must obviously adopt a full quantum-mechanical point of view and describe the field in the cavity as a damped quantum-mechanical oscillator, initially in thermal equilibrium at a small temperature T and coupled at time $t=0$ to a small ensemble of inverted two-level atoms. We summarize here the results of such an analysis, to be published elsewhere, and we compare them with the results of the large atom number maser theory of this paper. We restrict ourselves, for the sake of simplicity, to the case of a single atom in a $T=0$ K cavity. If the cavity is resonant with the atomic transition, a periodic exchange of energy between the atom and the cavity tends to set in the rate of this energy exchange:

$$\Omega_1 = \frac{d}{\hbar}\left[\frac{2\hbar\omega}{\epsilon_0 \pi L w_0^2}\right]^{1/2} \tag{45}$$

corresponds to the Rabi-nutation frequency of the atomic dipole in the field of a single photon stored in the cavity. This rate has to be compared to the reciprocal of the cavity damping time $T_{\rm cav}^{-1} = (\pi c/fL)$. If $\Omega_1 > T_{\rm cav}^{-1}$, several oscillations can actually occur before the cavity is damped. This regime corresponds to the oscillatory behavior of the large atom number maser case (see Sec. II). The condition $\Omega_1 > T_{\rm cav}^{-1}$ does indeed reduce to

$$f^2 > \frac{c}{\Gamma\mu L} \tag{46}$$

and is, within a numerical factor of the order of unity, identical to condition (27) with N_0 being replaced by one.

If, on the other hand, $\Omega_1 < T_{\rm cav}^{-1}$, the "atom + cavity" system is overdamped and the atomic energy irreversibly decays into the radiation field. The rate of atomic energy loss is, in this case, equal to $\Omega_1^2 T_{\rm cav} = f\Gamma\mu$, which again corresponds to the limit of the damped Rydberg-maser characteristic rate T_R^{-1} for $N_0 = 1$. This cavity induced-atomic damping will be observable only if it occurs faster than the atom escape time T_t^*, i.e., if $(f\Gamma\mu)^{-1}$ is smaller than T_t^* which can be expressed as

$$f > \frac{1}{\Gamma\mu T_t^*} . \tag{47}$$

This equation is the counterpart for $N=1$ of the threshold condition (40). In fact, for the Rydberg transition and the cavity μ factors we are considering in this paper, conditions (46) and (47) both correspond to critical finesses of the order of 10^5. This means that, as soon as the threshold will be reached, the one-atom maser will practically operate in the *oscillatory regime.*

Such an oscillatory energy exchange between a two-level atom and a cavity has a very simple quantum-mechanical explanation. The atom + cavity system behaves indeed as a compound "two-level" system. It can be either in the $|nS_{1/2};0\rangle$ state corresponding to an excited atom with no photon present or in the $|n\pm 1P_{1/2};1\rangle$ state corresponding to the atom in the lower level of the transition with one photon stored in the cavity. The coupling between these two states, equal to Ω_1 is responsible for the predicted quantum-mechanical oscillation. This one-atom version of the Rydberg maser would thus amount to preparing and studying a single atom and a single photon periodically exchanging their energy in a microwave cavity, certainly a new and interesting situation in the field of quantum electrodynamics. Experiments to observe and study this effect are presently under way in our laboratory.

Note added in proof. After this paper had been sent for publication, we have observed much lower thresholds ($N_0 \sim 100$ with cavity finesse $f \sim 3000$).

ACKNOWLEDGMENT

This work was supported in part by Direction des Recherches, Etudes et Techniques Grant No. 80/187.

*Permanent address: Laboratore Fizica Atomica e Molecolare, via del Giardino 3, 56100 Pisa, Italy.

[1]R. H. Dicke, Phys. Rev. 93, 99 (1954).

[2]M. Gross, P. Goy, C. Fabre, S. Haroche, and J. M. Raimond, Phys. Rev. Lett. 43, 343 (1979).

[3]S. Haroche, C. Fabre, P. Goy, M. Gross, and J. M. Raimond, *Laser Spectroscopy IV,* edited by H. Walther and K. W. Rothe (Springer, Berlin 1979), p. 244.

[4]L. Moi, C. Fabre, P. Goy, M. Gross, S. Haroche, P. Encrenaz, G. Beaudin, and B. Lazareff, Opt. Commun. 33, 47 (1980).

[5]S. Haroche, in *Atomic Physics 7,* edited by D. Kleppner and F. Pipkin (Plenum, New York, 1980).

[6]R. Bonifacio and L. A. Lugiato, Phys. Rev. A 11, 1507 (1975); 12, 587 (1975); R. Bonifacio, P. Schwendimann, and F. Haake, *ibid.* 4, 302 (1971); 4, 854 (1971).

[7]M. Gross, Thèse d'Etat, Université Paris VI, 1980 (unpublished); M. Gross and S. Haroche, Phys. Rep. (in press).

[8]A. Crubellier, S. Liberman, and P. Pillet, Phys. Rev. Lett. 41, 1237 (1978).

[9]N. E. Rehler and J. H. Eberly, Phys. Rev. A 3, 1735 (1971).

[10]D. C. McGillivray and M. S. Feld, Phys. Rev. A 14, 1169 (1976).

[11]V. De Giorgio, Opt. Commun. 2, 262 (1971).

[12]F. Haake, H. Kings, G. Schröder, J. Hauss, and R. Glauber, Phys. Rev. A 20, 2047 (1979).

[13]D. Polder, M. Schuurmans, and Q. Vrehen, Phys. Rev. A 19, 1192 (1972).

[14]R. Friedberg, S. R. Hartmann, and J. T. Manassah, Phys. Lett. A40, 365 (1972); R. Friedberg and S. R. Hartmann, Phys. Rev. A 10, 1728 (1974).

[15]T. Arecchi and E. Courtens, Phys. Rev. A 2, 1730 (1970).

[16]A. Crubellier, S. Liberman, and P. Pillet, Opt. Commun. 33, 143 (1980).

[17]P. Goy, C. Fabre, M. Gross, and S. Haroche, J. Phys. B 13, L-83 (1980).

[18]J. M. Raimond, G. Vitrant, and S. Haroche, J. Phys. B 14, L-655 (1981).

[19]P. Goy and B. Castaing, Phys. Rev. B 7, 4409 (1973).

[20]C. Fabre, P. Goy, and S. Haroche, J. Phys. B 10, L-183 (1977).

[21]T. Jeys, G. Foltz, K. Smith, E. Beiting, F. Kellert, F. Dunning, and R. Stebbings, Phys. Rev. Lett. 44, 390 (1980).

[22]C. Fabre, S. Haroche, and P. Goy, Phys. Rev. A 18, 229 (1978); 22, 778 (1980).

[23]See note added in proof.